Tectonophysics, 78 (1981) 1—21
Elsevier Scientific Publishing Company, Amsterdam — Printed in The Netherlands

FABRIC ANALYSIS BY ORIENTATION DISTRIBUTION FUNCTIONS

H.J. BUNGE

Institut für Metallkunde und Metallphysik, Technische Universität, Clausthal (F.R. of Germany)

(Received January 26, 1981)

ABSTRACT

Bunge, H.J., 1981. Fabric analysis by orientation distribution functions. In: G.S. Lister, H.-J. Behr, K. Weber and H.J. Zwart (Editors), The Effect of Deformation on Rocks. Tectonophysics, 78: 1—21.

Crystalline materials (natural or artificial) may consist of several phases (minerals) the crystal structures and relative amounts of which will generally be known. In order to fully characterize such a material, also the form and spatial distribution of the phases, the grain structure, and lattice defects and their distribution must be specified by appropriate distribution functions. Among these, the Orientation Distribution Function (texture, fabric structure) plays an important role. It can be deduced from experimental pole figures by series expansion methods. In textured materials two different symmetries can be distinguished, the crystal symmetry and the statistical sample symmetry. Special consideration must be given to the inversion centre as an element of either of these symmetries and in Friedels' law. A complete description of all possible sample symmetries can be given in terms of black—white symmetry groups. The determination of the odd part of the texture function is strongly related to these groups and the various kinds of the inversion centre. Each combination of a certain crystal symmetry group with a certain sample symmetry group induces a certain space group in the orientation space, the proper consideration of which minimizes the required amount of numerical calculations. The texture function (ODF) is the most important factor in the relation between anisotropic properties of single crystals and the polycrystalline material. Changes of the ODF can be used as a sensitive indicator for solid state processes having occurred in the material.

DEFINITION OF THE FABRIC STRUCTURE

Natural rocks as well as artificial materials, e.g. metals, ceramics and polymers, may consist of one or more minerals or phases, the crystal structures and relative amounts of which will generally be known. This does, however, by no means characterize the material sufficiently. Rather it is necessary to additionally specify its fabric structure i.e.:

(1) The spatial distribution of the phases.

(2) The composition of the phases of individual crystallites.

(3) Deviations of the crystallites from the ideal crystal structure.

This is illustrated in Fig. 1.

0040-1951/81/0000—0000/$02.50

Single phase materials

In the following we shall only deal with the second feature, i.e. the grain structure of a single phase material consisting of crystallites of ideal structure. A material of this type is fully specified by the grain boundary network and the orientation of the crystallographic axes of all grains, Fig. 2. In order to assess the macroscopic properties of such a material it is generally not necessary and not even desirable to describe individual grains of the material. Besides this, a grain-by-grain description is usually not feasible. Rather, the fabric will be described by certain statistical distribution functions e.g.:

(1) The orientation distribution function.
(2) The grain size (and its distribution).
(3) The grain shape (and its distribution).
(4) The orientation correlation (across the grain boundaries).

The parameters 2—4 are illustrated in Fig. 3 (Bunge, 1979). There are several variants of how to quantitatively define these parameters.

The orientation distribution function

Grain size, grain shape and orientation correlation may have considerable influence on the properties of the material. In the present, we shall, however, confine ourselves to the orientation distribution function i.e. the volume fraction of crystallites having the orientation g of their crystallographic axes with respect to a sample reference system:

$$dV(g)/V = f(g)\, dg \qquad (1)$$

This volume fraction is indicated in Fig. 4 by the shaded grain cross-sections.

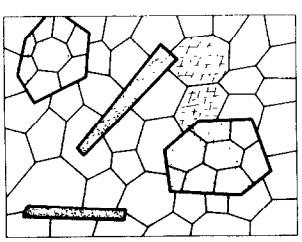

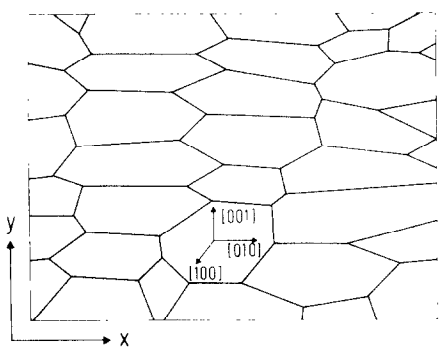

Fig. 1. Schematic structure of a polycrystalline, multiphase material containing lattice defects.

Fig. 2. A polycrystalline one-phase material is characterized by the orientation of the crystal axes of all grains and the grain boundary network.

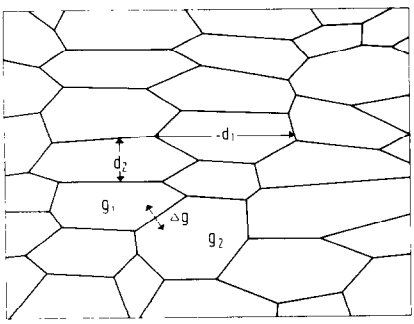

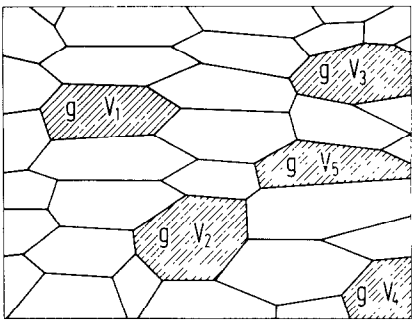

Fig. 3. Grain size, grain shape and orientation correlation (Bunge, 1979).

Fig. 4. The volume fraction $dV(g)$ of crystals having the orientation g within the limits of dg.

Definition of crystal orientation

The crystallographic orientation of a crystallite in a polycrystalline sample is defined by the orientation of a crystal-fixed coordinate system with respect to a sample-fixed reference system Fig. 5 (Bunge, 1969).

In particular, it can be specified in many different ways. In Fig. 6 (Bunge, 1979) one specific crystal direction $[hkl]$ has been chosen. Its orientation with respect to the sample coordinate system may be described by two angular coordinates $\alpha\beta$. The crystal is then left with one degree of freedom to rotate about $[hkl]$ which has to be specified by a third parameter γ. Another frequently used description of the relative orientation of two coordinate systems is the one by Eulerian angles shown in Fig. 7. It consists of three successive rotations about the crystal axes $Z'X'Z'$ starting from a position with the two coordinate systems parallel.

The orientation space

In any case, the full description of the orientation requires the specification of three parameters. The values of these parameters may be represented

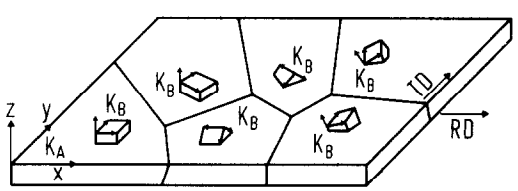

Fig. 5. The sample-fixed reference system K_A and the crystal-fixed coordinate system K_B (Bunge, 1979). *RD* and *TD* are rolling direction and transverse direction respectively, in a rolled sheet.

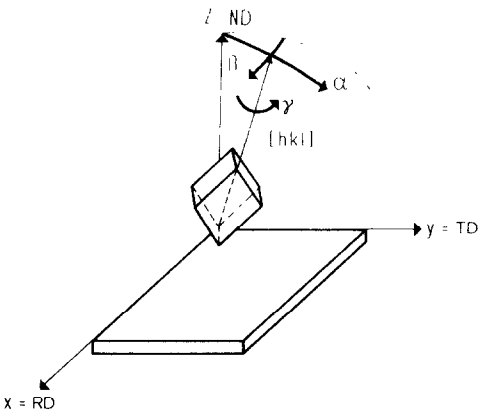

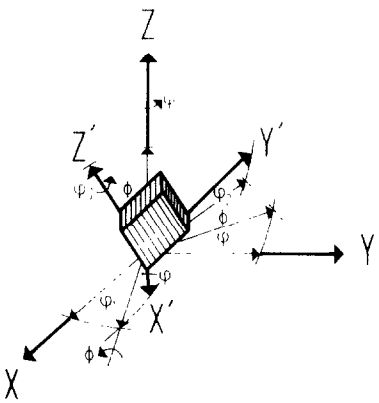

Fig. 6. The orientation of a crystallite may be specified by the polar coordinates $\alpha\beta$ of a specific crystal direction $[hkl]$ with respect to the sample coordinate system and the angle γ of a rotation about $[hkl]$ (Bunge, 1979).

Fig. 7. The Eulerian angles are defined by three successive rotations through φ_1 about Z', ϕ about X' and φ_2 about Z', starting from a position with the two coordinate systems parallel.

by a point in a three-dimensional space, the orientation space. In Fig. 8 the Eulerian angles have been chosen and have been represented as rectangular Cartesian coordinates. Hence, the orientation distribution function is a function of three variables which may be represented in the three dimensional space of Fig. 8:

$$f(g) = f(\varphi_1\phi\varphi_2) = f(\alpha\beta\gamma) = \ldots \quad (2)$$

DETERMINATION OF THE ORIENTATION DISTRIBUTION FUNCTION

Individual orientation measurements

In certain cases it is possible (e.g. by universal stage measurements, by Laue-photographs, by electron diffraction) to individually measure the orientations of all crystallites of a sample. Each crystallite is then represented by a point in the orientation space. An example is shown in Fig. 9 according to Wenk and Wilde (1972).

Accumulating measurements (pole figures)

Frequently, however, the measurement of a large number of individual crystallites will be too time-consuming. In these cases an accumulating method can be used. In Fig. 10 the principles of X-ray diffraction in a polycrystalline sample are shown. After certain corrections (e.g. back-ground

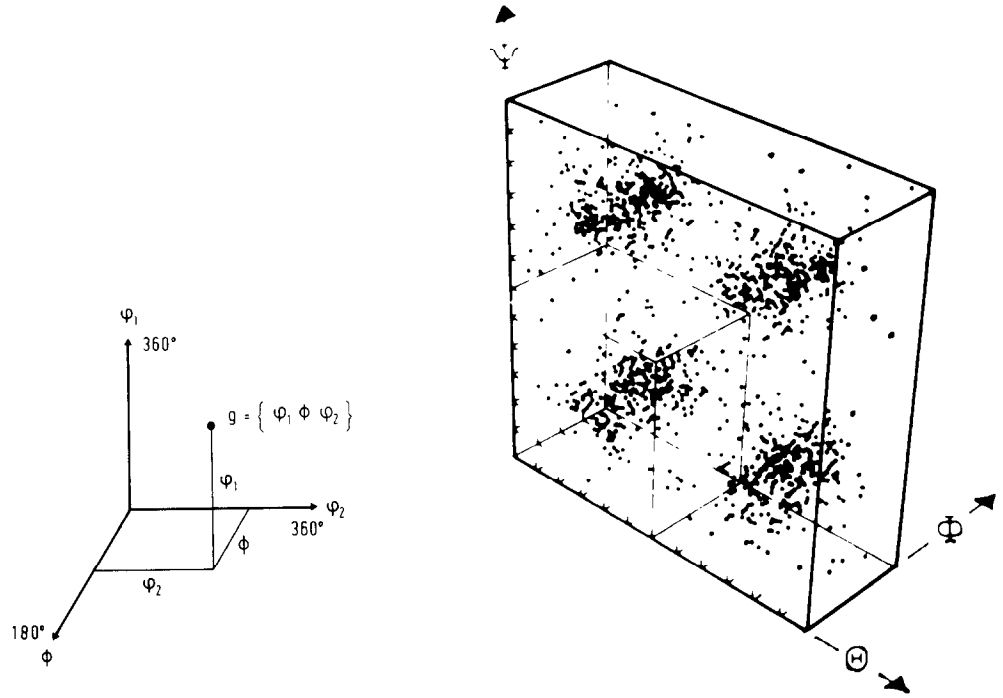

Fig. 8. An orientation *g* of a crystallite may be specified by a point in a three-dimensional space, the orientation space.

Fig. 9. The orientations of individual crystallites of a Yule marble sample represented in the space of the Eulerian angles Ψ-Φ according to Wenk and Wilde (1972). (The definition of the Eulerian angles Ψ-Φ is slightly different from that used in Fig. 7).

scattering, absorption, defocalization) the measured intensity is proportional to the volume fraction of crystals in reflection position. This method accumulates the reflected intensities of all crystals which have a particular [*hkl*]-direction in a specific orientation with respect to the sample reference system Fig. 11a. By rotating the sample through two independent angles, all possible positions of [*hkl*] with respect to the sample coordinate system can be registered. The so obtained intensity distribution function is the well-known (*hkl*)-fabric diagram (Sander, 1950) or (*hkl*)-pole figure (Wassermann and Grewen, 1962) Fig. 11b *. As can be seen in Fig. 11, the pole figure is not changed if all crystals are arbitrarily rotated about the [*hkl*]-direction.

* Note that pole figures are usually characterized by the Miller indices of the reflecting lattice *plane* (*hkl*) whereas the definition of the orientation described in Fig. 6 refers to a specific crystal *direction* [*h'k'l'*], i.e. the normal direction to the plane (*hkl*).

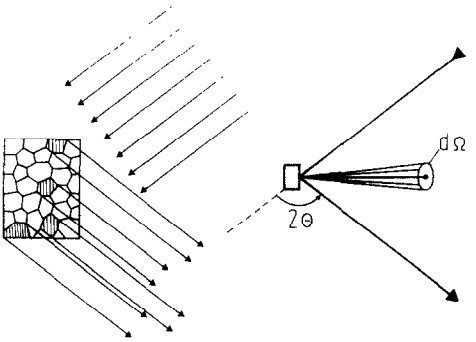

Fig. 10. Crystallites, the direction [*hkl*] of which falls into the solid angle element dΩ, are in reflecting position to the incident X-ray beam. The intensity of the reflected beam is proportional to the volume fraction of these crystals.

The pole figure is thus an integral over the third orientation parameter:

$$P_{hkl}(\alpha\beta) = \frac{1}{2\pi}\int f(\alpha\beta\gamma)\,\mathrm{d}\gamma \tag{3}$$

It does not contain the full information about the orientation distribution of the crystallites. The missing information may be provided by reflecting the X-rays from other lattice planes ($h'k'l'$). This gives rise to similar relations as eq. 3 with other orientation parameters.

Solutions of the fundamental relation

The fundamental problem in texture analysis is to solve the integral equation (eq. 3) for the function $f(\alpha\beta\gamma)$ if several different pole figures i.e. two-

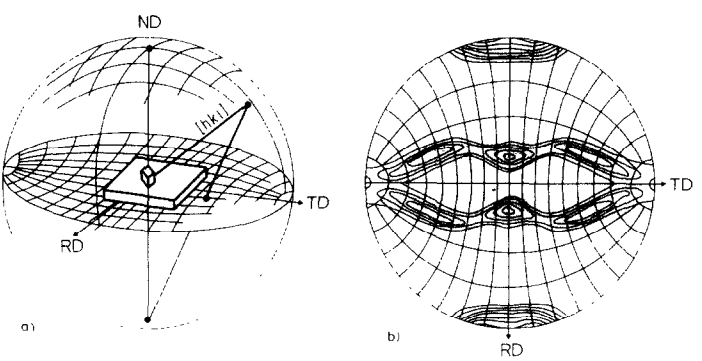

Fig. 11. The orientation of the direction [*hkl*] of an individual crystallite with respect to the sample reference system and the pole distribution function, i.e. (*hkl*) fabric diagram or (*hkl*) pole figure (Bunge, 1979).

dimensional projections of it are known. Several methods of how to achieve the solution have been proposed. The first idea is to replace the integral by a sum and thus to obtain a system of linear equations instead of a system of integral equations (Williams, 1968). This method has been designated as vector method (Ruer and Baro, 1977). Recently an integral inversion formula has been proposed by Matthies (1979).

A fourth method is the series expansion method which has found the widest use thus far (Bunge, 1965, 1969; Roe, 1965). In the following we shall deal with this method only.

The series expansion method

A solution to the above mentioned problem may be achieved by developing both functions the distribution function $f(\alpha\beta\gamma)$ and the pole figures $P_{hkl}(\alpha\beta)$ into series whereby the function f will be expressed in Eulerian angles $f(\varphi_1\phi\varphi_2)$:

$$f(\varphi_1\phi\varphi_2) = \sum_{l=0}^{\infty} \sum_{m=-l}^{+l} \sum_{n=-l}^{+l} C_l^{mn} T_l^{mn}(\varphi_1\phi\varphi_2) \tag{4}$$

$$P_{hkl}(\alpha\beta) = \sum_{l=0}^{\infty} \sum_{n=-l}^{+l} F_l^n(hkl)\, k_l^n(\alpha\beta) \tag{5}$$

where $k_l^n(\alpha\beta)$ are spherical harmonics and $T_l^{mn}(\varphi_1\phi\varphi_2)$ are generalized spherical harmonics. These are mathematically known functions the properties of which need not be discussed here. Inserting eqs. 4 and 5 into the fundamental relation, eq. 3, yields a relation between the coefficients F_l^n of the experimental functions and the ones C_l^{mn} of function which is to be determined:

$$F_l^n(hkl) = \frac{4\pi}{2l+1} \sum_{m=-l}^{+l} C_l^{mn} k_l^{*m}(hkl) \tag{6}$$

If the F_l^n are known for sufficiently many pole figures (hkl) the system of linear equations, eq. 6, can be solved for the coefficients C_l^{mn}. The coefficients $F_l^n(hkl)$ can be obtained from the experimentally measured pole figures $P_{hkl}(\alpha\beta)$ by the inversion of eq. 5 which reads:

$$F_l^n(hkl) = \int P_{hkl}(\alpha\beta)\, k_l^{*n}(\alpha\beta)\, \mathrm{d}\Omega \tag{7}$$

i.e. an integral taken over the whole pole sphere of the measured function multiplied by the corresponding spherical harmonic. Hence, when the coefficients $F_l^n(hkl)$ have been calculated according to eq. 7 then eq. 6 can be solved for the C_l^{mn} and finally the orientation distribution function $f(\varphi_1\phi\varphi_2)$ can be calculated for any required values of $\varphi_1\phi\varphi_2$ by summing up eq. 4.

Representation of the results

Usually the function $f(\varphi_1\phi\varphi_2)$ will be needed in the complete range of orientation parameters $\varphi_1\phi\varphi_2$. The calculations will thus be carried out in steps $\Delta\varphi_1\Delta\phi\Delta\varphi_2$ (say 5° each). The result may be interpolated by equidensity lines as is shown for φ_1 = const. in Fig. 12. This may be done for all sections in steps of $\Delta\varphi_1$ to span the whole range of the orientation space, Fig. 13 (Bunge et al., 1974). The sections φ_1 = const. may be stacked one upon the other, connecting the level lines to level surfaces as is shown in Fig. 14 (only one of the level surfaces is shown). The n-th level surface thus contains the points $\varphi_1\phi\varphi_2$ such that:

$$f(\varphi_1\phi\varphi_2) = n \cdot f_r \tag{8}$$

where f_r is the orientation density of the random distribution.

THE INFLUENCE OF SYMMETRIES

Crystal symmetries

The formulae eqs. 4—7 are valid for triclinic crystals. If the crystal symmetry is higher, then special symmetry-adapted functions can be used (Bunge, 1969) instead of the functions T_l^{mn} and k_l^n in eqs. 4 and 5. This reduces the number of terms in eq. 6, i.e. the number of unknown coefficients which are to be determined by solving this system of equations. The number of unknowns, in turn, determines the necessary number of equations and hence the number of different pole figures needed in order to uniquely solve eq. 6. These numbers (as a function of the degree l) are shown in Fig. 15 for the various crystal symmetries (Bunge, 1969). The lower the symmetry and the higher the required degree l of the series expan-

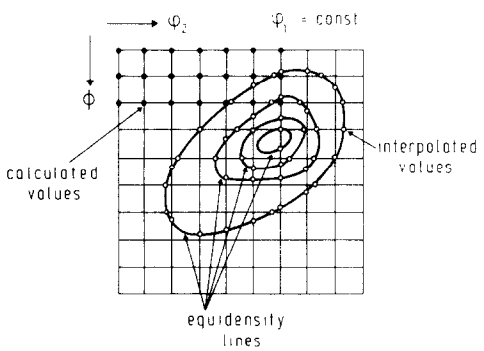

Fig. 12. The function $f(\varphi_1\phi\varphi_2)$ has been calculated in steps $\Delta\varphi_1\Delta\phi$. The so obtained functional values have been linearly interpolated to find the intersection of a certain level line with the coordinate lines.

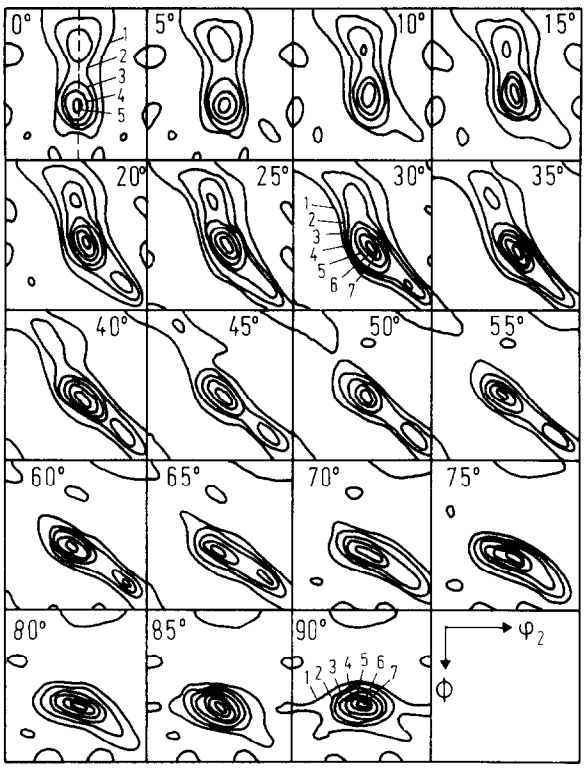

Fig. 13. The sections $\varphi_1 = n \cdot 5°$ of the texture of a cold-rolled and recrystallized iron sheet (Bunge et al., 1974).

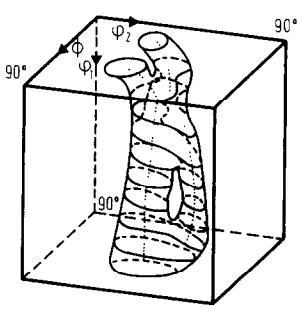

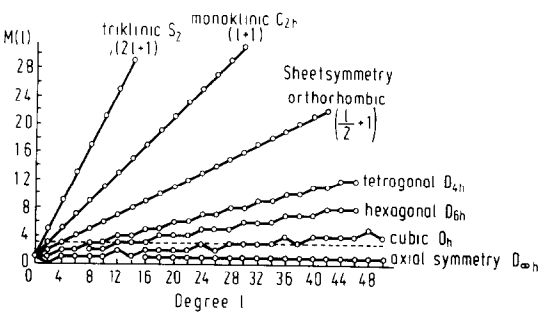

Fig. 14. The level lines $f = 4 \cdot f_r$ of the texture of Fig. 13 have been stacked three-dimensionally and have been connected to the level surface (Bunge et al., 1974).

Fig. 15. The number of linearly independent spherical harmonics of order l for the various crystal symmetries (Bunge, 1969).

sion the higher is the number of pole figures needed to determine the orientation distribution function.

The centre of inversion

Special consideration must be given to the centre of inversion. If the crystals belong to a non-centrosymmetric group then they may exist in a right- and left-handed form (Fig. 16) and these may be present in a polycrystalline sample with a different volume fraction M^R and M^L (Fig. 17). Hence, the sample may be considered as a two-phase material consisting of a right-handed and a left-handed phase. The two phases may have independent orientation distribution functions $f^R(g)$ and $f^L(g)$ which may be expressed by series expansions according to eq. 4 with coefficients $(C^R)_l^{mn}$ and $(C^L)_l^{mn}$. In a polycrystal diffraction experiment according to Fig. 10 corresponding crystal directions of right-handed and left-handed crystals cannot be distinguished. The corresponding pole figures are always superposed. Hence, the distribution functions $f^R(g)$ and $f^L(g)$ cannot be determined separately. Rather, a mixed texture function $f(g)$ will be obtained with the coefficients:

$$\tilde{\tilde{C}}_l^{mn} = M^R(C^R)_l^{mn} + M^L(C^L)_l^{mn} \qquad \text{for } l \text{ even} \qquad (9)$$

$$\tilde{\tilde{C}}_l^{mn} = M^R(C^R)_l^{mn} - M^L(C^L)_l^{mn} \qquad \text{for } l \text{ odd} \qquad (10)$$

A centrosymmetric crystal may be considered as right-handed and left-handed *at the same time*. Hence, the volume fractions M^R and M^L must be equal and the orientation distribution of the right-handed and left-

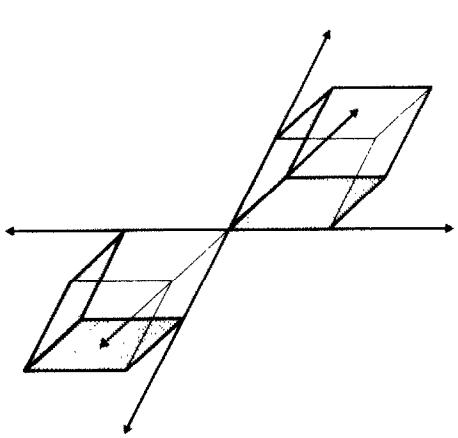

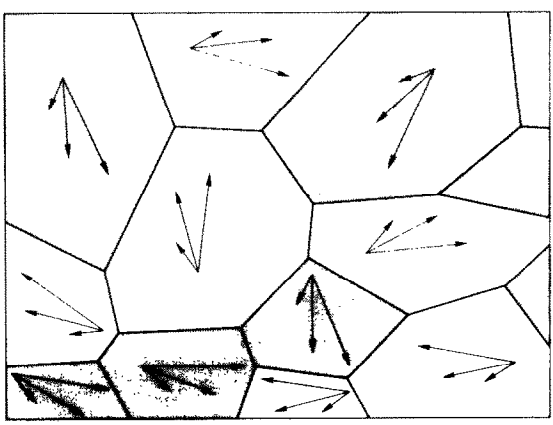

Fig. 16. Right- and left-handed crystal forms.

Fig. 17. A polycrystalline sample of non-centrosymmetric crystals consisting of right- and left-handed crystal forms.

handed crystals and hence the coefficients $(C^{\mathrm{R}})_l^{mn}$ and $(C^{\mathrm{L}})_l^{mn}$ must be the same. Thus, it follows for centrosymmetric crystals:

$$\tilde{C}_l^{mn} = (C^{\mathrm{R}})_l^{mn} = (C^{\mathrm{L}})_l^{mn} \qquad \text{for } l \text{ even} \tag{11}$$

$$\tilde{C}_l^{mn} = 0 \qquad \text{for } l \text{ odd} \tag{12}$$

This means, the coefficients $\tilde{C}_l^{mn}$ of the experimentally determined texture are equal with the true ones $(C^{\mathrm{R}})_l^{mn}$ and $(C^{\mathrm{L}})_l^{mn}$ (in the right- or left-handed description) only for the even values of l whereas the true coefficients $(C^{\mathrm{R}})_l^{mn}$ or $(C^{\mathrm{L}})_l^{mn}$ for odd values of l cannot be determined experimentally from pole figures.

In non-centrosymmetric crystals a centre of inversion is induced artificially by X-ray diffraction (Friedels' law) which makes the direction $[hkl]$ indistinguishable of $[\bar{h}\,\bar{k}\,\bar{l}]$. Hence, the (hkl) pole figure is always superposed with the $(\bar{h}\,\bar{k}\,\bar{l})$ pole figure. This may be considered as if to the right-handed phase a *hypothetical* left-handed one is being added with the same volume fraction and the same texture. Hence, even if only right-handed crystals were present eqs. 11 and 12 are valid. This means, the coefficients of odd order of the texture function cannot be obtained directly from polycrystal diffraction experiments (unless anomalous scattering is used).

The odd part of the texture function

Because of eqs. 11 and 12 it is necessary to consider the terms of even and odd l in eq. 4 separately, thus, splitting the distribution functions into an even and odd part:

$$f(g) = f^{\mathrm{even}}(g) + f^{\mathrm{odd}}(g) \geqslant 0 \tag{13}$$

According to the definition eq. 1, $f(g)$ is the volume fraction of crystals in the orientation g. This volume fraction cannot be negative. It can, however, be zero in a certain region Z^0 of the g-space. This region can be concluded directly from the zero-regions of the pole figures (an orientation g, the (hkl) pole of which falls into the zero-region of the (hkl) pole figure must belong to the zero-region in the g-space). Hence, it is:

$$f^{\mathrm{odd}}(g) = -f^{\mathrm{even}}(g)\,, \qquad \text{in } Z^0 \tag{14}$$

where $f^{\mathrm{even}}(g)$ has been calculated according to the method mentioned above. If, thus, $f^{\mathrm{odd}}(g)$ is known in the region Z^0 it can there be approximated by a series (eq. 4) with odd terms only according to the condition (Bunge and Esling, 1979):

$$\left[f^{\mathrm{odd}}(g) - \sum_{l=1(2)}^{L} \sum_{m=-l}^{+l} \sum_{n=-l}^{+l} C_l^{mn} T_l^{mn}(g) \right]^2 \mathrm{d}g = \mathrm{Min} \tag{15}$$

The so obtained coefficients C_l^{mn} of odd order l define an approximation to the function $f^{odd}(g)$ in the *whole* range of g. In the case that there is a zero-region in the function $f(g)$, it is thus possible to determine also the odd part of the orientation distribution function from pole figure measurements.

It is to be mentioned, that the restrictions concerning the odd part of the orientation distribution function are due to polycrystal measurements. They are thus inherent in all methods of solving the fundamental relation eq. 3. But they do not occur with individual orientation measurements such as were shown in Fig. 9. The interpolation of the point distribution Fig. 9 by a continuous distribution function (Bunge, 1969) thus allows to determine the odd coefficients in a more straightforward way.

The statistical sample symmetry

Besides the crystal symmetry, there may be another kind of symmetry in polycrystalline samples, namely the sample symmetry (cf. Weissenberg, 1922; Shubnikov, 1958; Paterson and Weiss, 1961). It relates crystallographically well distinguished crystal orientations with one another in such a way that these orientations occur with equal volume fraction in the sample. In Fig. 18 for example two different crystal orientations are shown which are related to one another by a two-fold axis parallel to the rolling direction of a metal sheet. If *all* crystal orientations bearing this relationship occur with equal volume fractions then the sample is said to exhibit a two-fold axis as an element of the sample symmetry (as is easily seen in Fig. 18 this axis is not an element of the crystal symmetry). The sample symmetry reduces the number of different values that can be taken on by the index n in a similar way as the crystal symmetry reduces the number of values which the index m may take on (see Fig. 15).

Again special consideration must be given to the inversion centre. We consider non-centrosymmetric crystals. The most obvious way of achieving a centrosymmetric sample is to add a left-handed crystal in the centrosymmetric position to a right-handed one and vice-versa as was shown in Fig. 16.

If the sample direction y contains the direction $[hkl]$ (of a right-handed crystal) then the sample direction $-y$ contains also the direction $[hkl]$ (although of a left-handed crystal). Hence, the sample directions $+y$ and $-y$ are indistinguishable from the point of view of crystallographic directions falling into them.

There is, however, still another possibility of achieving a centrosymmetric sample with *only* right-handed (or *only* left-handed) crystals present in the sample. To a crystal having its $[hkl]$-direction parallel to the sample direction y, we add another one (of the same form) having its $[hkl]$-direction parallel to $-y$. If this relation holds for *all* sample directions y and *all* crystal directions $[hkl]$ then the sample direction $-y$ is indistinguishable of the sample direction $+y$, the sample thus being centrosymmetric. This is, however, a different (and more complex) kind of centrosymmetry compared with the first one.

Black-white point group

If we designate the [*hkl*]-direction of a right-handed crystal by a black point in the stereographic projection and the corresponding [*hkl*]-direction of a left-handed crystal by a white point then the following four symmetries shown in Fig. 19 are possible. Rotation axes as shown in Fig. 18 transfer white points into white ones and black points into black ones. Hence, the sample symmetry is to be described by black—white point groups rather than by the ordinary ones (Shubnikov and Belov, 1964).

Symmetries in the Euler space

Because of the crystal symmetry as well as the sample symmetry, points in the orientation space with different Eulerian angles will have the same functional value of the orientation distribution function Fig. 20. Since the Eulerian angles are periodical variables the orientation distribution function is a three-dimensionally periodical function. If it exhibits additional symmetries such as shown in Fig. 20 this will induce a certain space group in the Euler space and possibly reduce the unit cell and asymmetric unit as is shown in Fig. 21 for cubic crystal symmetry and orthorhombic sample symmetry and in Fig. 22 (Baker, 1970) for trigonal crystal and monoclinic sample symmetry. The appropriate consideration of these space groups may considerably reduce the amount of computational work needed when calculating the orientation distribution function.

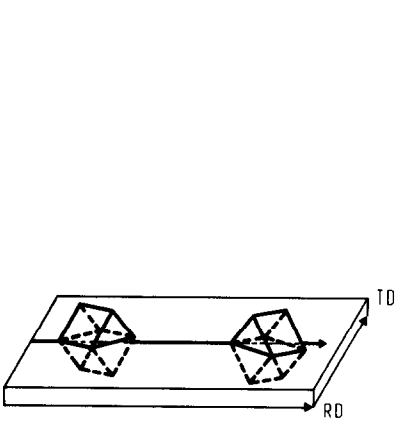

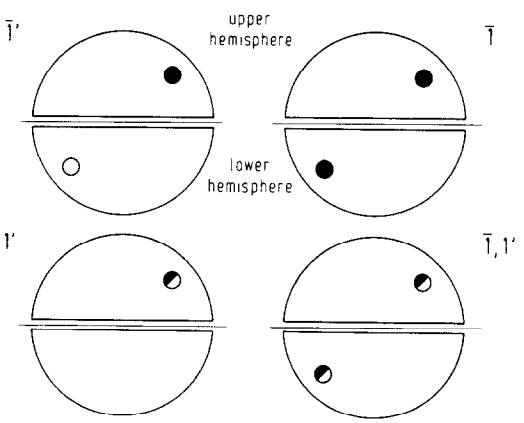

Fig. 18. A two-fold axis parallel to the sample direction *RD* (rolling direction) transfers any crystal orientation into another one which occurs with equal volume fraction in the sample. *TD* = transverse direction.

Fig. 19. Four possible symmetries among right-handed (black) and left-handed (white) crystals.

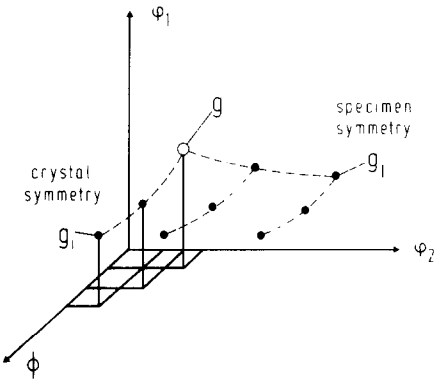

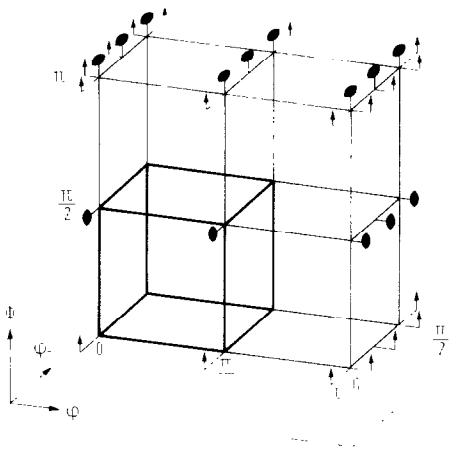

Fig. 20. Orientations related by the sample symmetry and the crystal symmetry.

Fig. 21. Space group $P\frac{2}{\phi}\frac{2}{m}\frac{2}{\phi}$ in the Euler space corresponding to cubic crystal symmetry and orthorhombic sample symmetry.

EVALUATION OF THE RESULTS

The method described above answers the question which volume fraction of the sample has a crystallographic orientation g described by the Eulerian angles $\varphi_1\phi\varphi_2$. The result is contained in the distribution chart Fig. 13 and may be read from it for any desired crystal orientation. The Eulerian angles

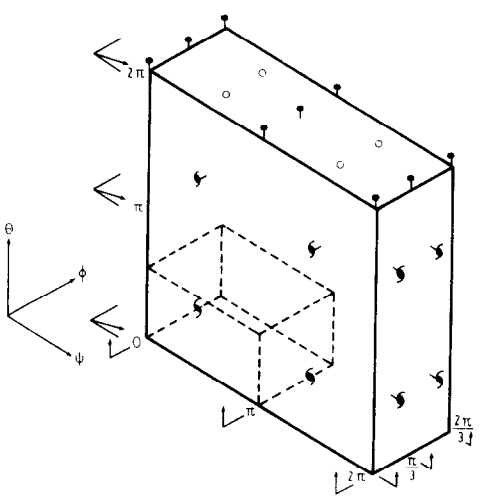

Fig. 22. Space group $P\frac{2}{\theta}\frac{2}{n}\frac{2}{\theta}$ in the Euler space corresponding to trigonal crystal symmetry and monoclinic sample symmetry (Baker, 1970).

as orientation coordinates are convenient for the mathematical calculations. In general, however, the crystallographer is more familiar with describing orientations by poles in a stereographic projection whereby the plane of projection may either be fixed to the sample reference system (pole-chart or pole figure) or to the crystal reference system (axis chart or inverse pole figure). Hence, a transformation from Eulerian angles into these better known orientation parameters will be disirable. It can easily be achieved from the definition of Eulerian angles by three successive rotations about fixed axes Fig. 23. These rotations may easily be carried out by the well-known "rolling" operation in the stereographic projection. In Fig. 24 the crystallographic directions $X' = [100]$, $Y' = [010]$, and $Z' = [001]$ are shown in a projection fixed to the sample reference system (rolling plane of sheet). Fig. 25 gives the inverse representation, namely the sample reference axes $X = RD$, $Y = TD$, $Z = ND$ projected into the crystal (001)-plane. From these reference points the position of any other crystal direction (in Fig. 24) or any other sample direction (in Fig. 25) can easily be constructed by well-known methods. The coordinate transformation from Eulerian angles to

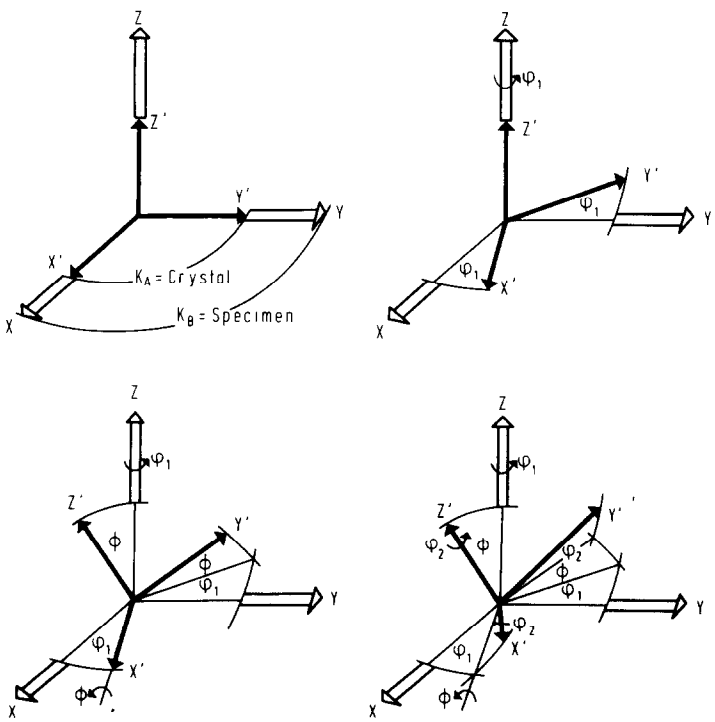

Fig. 23. The Eulerian angles are defined by three successive rotations: (1) about the crystal Z'-axis through φ_1; (2) about the crystal X'-axis through ϕ; and (3) about the crystal Z'-axis through φ_2.

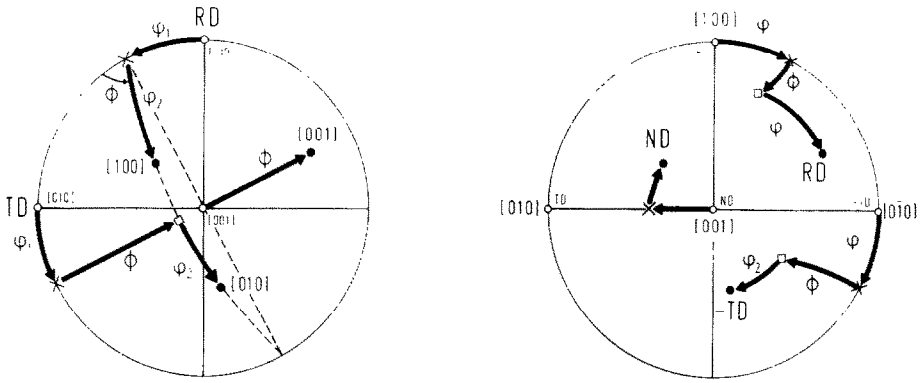

Fig. 24. The positions of the crystal reference directions $X' = [100]$, $Y' = [010]$, $Z' = [001]$ in a sample-fixed stereographic projection.

Fig. 25. The positions of the sample reference directions $X = RD$, $Y = TD$, $Z = ND$ in a crystal-fixed stereographic projection.

poles can even be more facilitated by using prefabricated charts showing the low-index orientations of the representation Fig. 25 in the Euler space. Charts of this type are available thus far for cubic (Davies et al., 1971a; Jura et al., 1976) and hexagonal (Davies et al., 1971b) crystal symmetry. These charts Fig. 26 can be put immediately on top of the distribution charts Fig. 12 or 13 and thus the corresponding orientation can be directly read off.

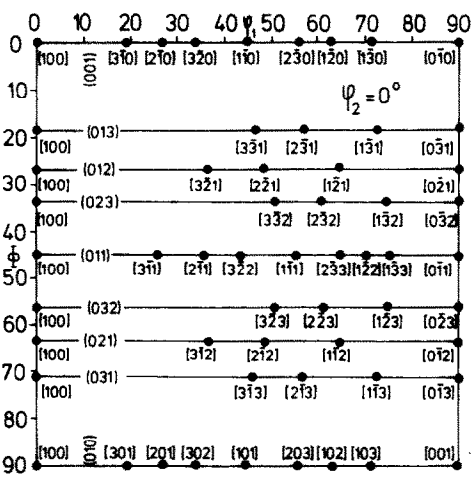

Fig. 26. Low-index orientations $RD \parallel [hkl]$ and $ND \parallel [uvw]$ according to Fig. 25 for cubic crystal symmetry (Jura et al., 1976).

Accuracy and limits of the method

The principle limit of accuracy of the method is given by the *statistical nature* of grains in a polycrystalline sample. This is to be seen in Fig. 9. The orientation density may be obtained by partitioning the whole orientation space into small boxes and counting the number N of points in them. The statistical error will thus be $\sqrt{N}$. Hence, the relative error of the orientation density brought about per definition by the statistical nature will be $1/\sqrt{N}$.

A *step scanning error* will arise from not measuring the pole figure as a continuous function. Usually a step scan of $5^\circ \times 5^\circ$ is being used. Hence, the resolving power of the method will not be better than 5°. Consequently, the steps $\Delta\varphi_1 \Delta\phi \Delta\varphi_2$ for the calculation of the function $f(\varphi_1 \phi \varphi_2)$ in Figs. 12—14 have been chosen as 5° too.

From eq. 6 it follows that the coefficients C_l^{mn} can no longer be uniquely determined if the number of pole figures (hkl) is smaller than the number of unknowns of this system of equations. As Fig. 15 shows, the number of unknowns increases with increasing degree l. Hence, there will be an upper limit l_{max} beyond which there is *no unique solution* for the function $f(g)$ with a given number of pole figures. This ambiguity is independent of the specific method of solving the equation (eq. 3).

A specific *ambiguity* is introduced if the odd part of the texture function is not determined (as was shown, the determination of the odd part needs special considerations). Because of this ambiguity one cannot distinguish between crystal directions $[hkl]$ and $[\bar{h}\,\bar{k}\,\bar{l}]$ falling into any sample direction. Hence, all sample symmetries are being interpreted as "grey" symmetries according to Fig. 19.

APPLICATIONS OF THE ORIENTATION DISTRIBUTION FUNCTION

Mean values of physical properties

One purpose for which the orientation distribution function is needed is the calculation of mean values of anisotropic physical properties. Young's modulus measured in a crystal direction $[hkl]$ (see Fig. 27) is a function of this direction, $E(hkl)$, which is shown for example in Fig. 28 for iron (Schmid and Boas, 1950). The Young's modulus of a polycrystalline sample in the sample direction y (Fig. 29; Bunge, 1979) may be obtained as the mean value over all crystals having their $[hkl]$ directions parallel to y multiplied by the volume fraction $A(hkl, y)$ of these crystals. Thus, it is (Bunge, 1969):

$$\bar{E}(y) = \int E(hkl) \cdot A(hkl, y)\, \mathrm{d}\Omega \qquad (16)$$

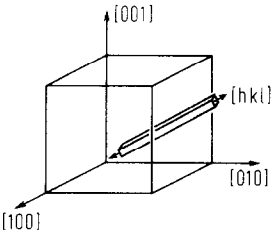

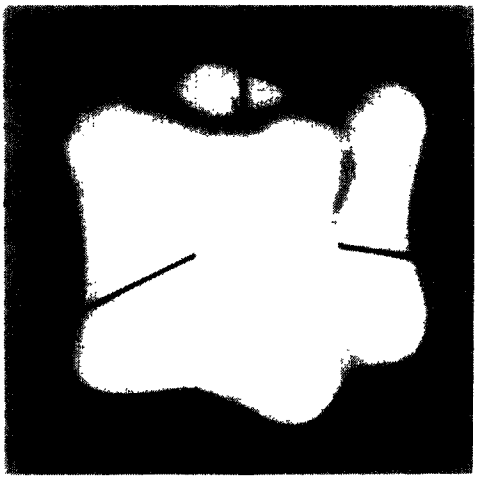

Fig. 27. Measuring Young's modulus in the crystal direction $[hkl]$.

Fig. 28. Young's modulus as a function of $[hkl]$ for iron (Schmid and Boas, 1950).

The volume fraction $A(hkl, y)$ is related to the orientation distribution function by:

$$A(hkl, y) = \int_{[hkl] \| y} f(\varphi_1 \phi \varphi_2) \, d\gamma \tag{17}$$

where the integral is to be taken over all those orientations the $[hkl]$-direction of which is parallel to y. Calculations of this type are needed in order to

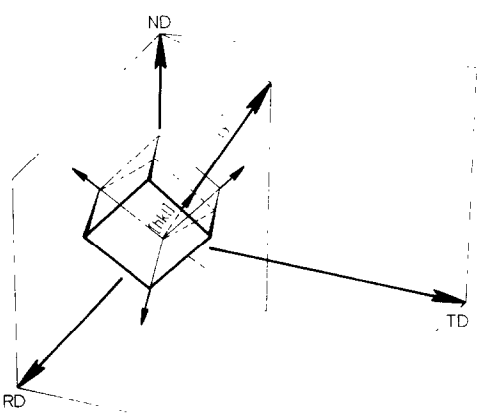

Fig. 29. A crystal in an orientation having the $[hkl]$-direction parallel to the sample direction y (Bunge, 1979).

rationalize anisotropic wave velocity in natural rocks (e.g. Kern and Fakhimi, 1975).

Comparison with model functions

The orientation distribution function $f(g)$ of a polycrystalline material may depend on a great number of influences having acted upon that sample during all of its history. In fact, it may depend on all processes capable of changing crystal orientation, e.g. plastic deformation, phase change, or recrystallization. Hence, the texture may be used as a sensitive indicator by which to follow these processes. In rock deformation it should be possible for instance, to use the texture as an indicator for the deformational history if only one had some model textures of known history. Such model textures may be obtained by *experimental* rock deformation (Siemes, 1977; Kern, 1979) or *theoretically* by calculating orientation changes after certain deformations according to some theories, e.g. the Taylor theory (Taylor, 1938). The comparison of the investigated texture with the model texture can, of course, be carried out in the pole figures (Lister, 1974). It will, however, be much more effective if the corresponding functions $f(g)$ can be compared because those functions are much more detailed and the comparison is therefore much more conclusive. Figure 30 shows the comparison of the experimental texture of a cold-rolled copper sheet with the theoretical texture calculated with the assumptions of the Taylor theory on the basis of {111} ⟨110⟩ glide (Bunge and Leffers, 1971).

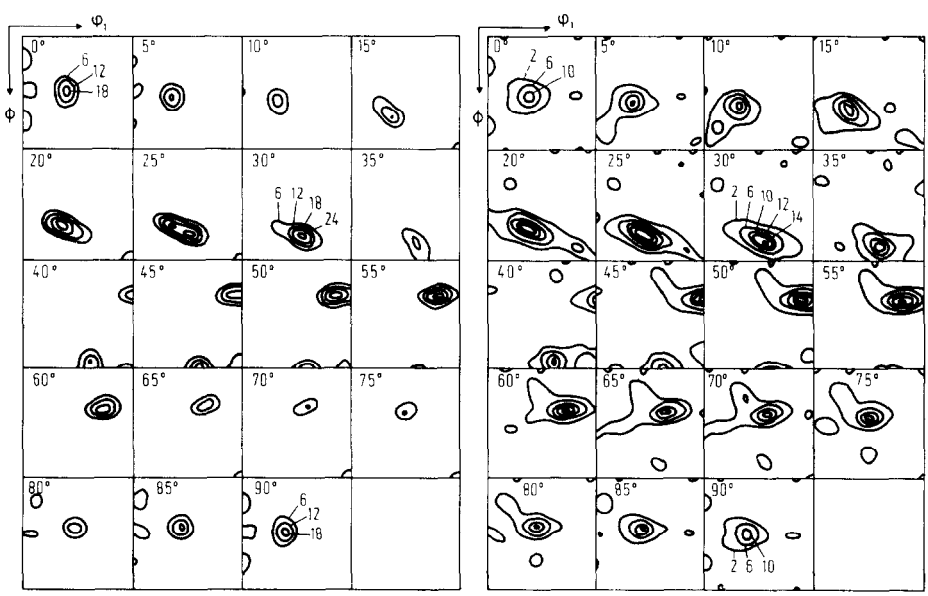

Fig. 30. Experimental texture of 90% cold rolled copper compared with the one calculated after the Taylor theory (Bunge and Leffers, 1971).

REFERENCES

Baker, D., 1970. On the symmetry of orientation distribution in crystal aggregates. Adv. X-Ray Anal., 13: 435—454.

Bunge, H.J., 1965. Zur Darstellung allgemeiner Texturen. Z. Metallkd., 56: 872—874.

Bunge, H.J., 1969. Mathematische Methoden der Texturanalyse. Akademie-Verlag, Berlin, 330 pp.

Bunge, H.J., 1977. Texture analysis by orientation distribution functions. Z. Metallkd., 68: 571—581.

Bunge, H.J., 1979. Textur und Anisotropie. Z. Metallkd., 70: 411—418.

Bunge, H.J. and Esling, C., 1979. Determination of the odd part of the texture function. J. Phys. (Paris), Lett., 40: 627—628.

Bunge, H.J. and Leffers, T., 1971. The three-dimensional orientation distribution obtained by computer simulation of the plastic deformation in face-centered cubic polycrystals. Scr. Metall., 5: 143—149.

Bunge, H.J., Schleusener, D. and Schläfer, D., 1974. Neutron-diffraction studies of the recrystallization textures in cold-rolled low-carbon steel. Met. Sci. J., 8: 413—423.

Bunge, H.J., Esling, C. and Muller, J., 1980. The role of inversion centre in texture analysis. J. Appl. Crystallogr., 13: 544—554.

Davies, G.J., Goodwill, D.J. and Kallend, J.S., 1971a. Charts for analysing crystallite distribution function plots for cubic materials. J. Appl. Crystallogr., 4: 67—70.

Davies, G.J., Goodwill, D.J. and Kallend, J.S., 1971b. Charts for analysing crystallite orientation distribution function plots for hexagonal materials. J. Appl. Crystallogr., 4: 193—196.

Gehlen, v., K., 1960. Die röntgenographische und optische Gefügeanalyse von Erzen, insbesondere mit dem Zählrohr-Texturgoniometer. Beitr. Mineral. Petrogr., 7: 340—388.

Jura, J., Pospiech, J. and Bunge, H.J., 1976. A standard System of FORTRAN programmes for three-dimensional texture analysis. Metallurgia (Cracow), 24: 111—176.

Kern, H., 1979. Texture development in calcite and quartz rocks deformed at uniaxial and real triaxial states of strain. Bull. Minéral., 102: 290—300.

Kern, H. and Fakhimi, M., 1975. Effect of fabric anisotropy on compressional-wave propagation in various metamorphic rocks for the range 20—700°C at 2 kbars. Tectonophysics, 28: 227—244.

Lister, G.S., 1974. The Theory of Deformation Fabrics. Thesis, Sidney.

Matthies, S., 1979. On the reproducibility of the orientation distribution function of texture samples from pole figures (Ghost phenomena). Phys. Status Solidi B, 92: K135—138.

Paterson, M.S. and Weiss, I.E., 1961. Symmetry concepts in the structural analysis of deformed rocks. Geol. Soc. Am. Bull., 72: 841—882.

Roe, R.J., 1965. Description of crystallite orientation in polycrystalline materials III General solution to pole figure inversion. J. Appl. Phys., 36: 2024—2031.

Ruer, D. and Baro, R., 1977. A new method for the determination of the texture of materials of cubic structure from incomplete reflection pole figures. Adv. X-Ray Anal., 20: 187—200.

Sander, B., 1950. Einführung in die Gefügekunde der geologischen Körper. Springer Verlag, Wien.

Schmid, E. and Boas, W., 1968. Plasticity of Crystals. Chapman and Hall, London.

Shubnikov, A.V., 1958. Etude des textures piezoélectriques. Dunod, Paris.

Shubnikov, A.V. and Belov, N.V., 1964. Colored Symmetry. Pergamon Press, Oxford.

Siemes, H., 1977. Fabric analysis and fabric development in ores. Geol. Fören. Stockholm Förh., 99: 172—185.

Taylor, G.I., 1938. Plastic strain in metals. J. Inst. Met., 62: 307—324.
Wassermann, G. and Grewen, J., 1962. Texturen metallischer Werkstoffe. Springer Verlag, Berlin, Göttingen, Heidelberg.
Wenk, H.R. and Wilde, W.R., 1972. Orientation distribution for three Yule marble fabrics. In: Flow and Fracture of Rocks. Geophys. Monogr., Am. Geophys. Union, 16: 83—94.
Weissenberg, K., 1922. Statistische Anisotropie in kristallinen Medien und ihre röntgenographische Bestimmung. Ann. Phys. 69, 409—435.
Williams, R.O., 1968. The representation of textures of rolled copper, brass and aluminium by biaxial pole figures. Trans. Met. Soc. AIME, 242: 105—115.